IEEE Photonics Journal
An IEEE Photonics Society Publication

Open Access

# Direct Generation of Subnanosecond Ince–Gaussian Modes in Microchip Laser

Volume 7, Number 1, February 2015

**Shuo Han**
**Yanqing Liu**
**Fang Zhang**
**Ying Zhou**
**Zhengping Wang**
**Xinguang Xu**

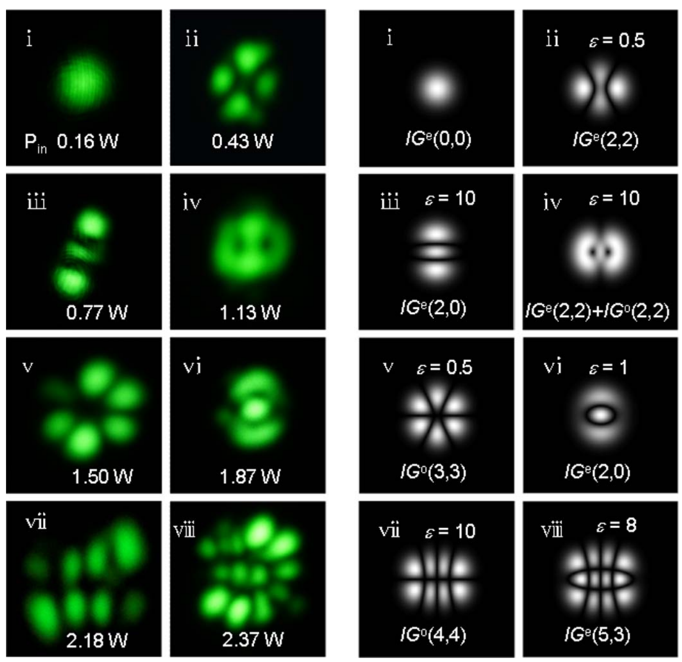


DOI: 10.1109/JPHOT.2015.2396905

# Direct Generation of Subnanosecond Ince–Gaussian Modes in Microchip Laser

**Shuo Han, Yanqing Liu, Fang Zhang, Ying Zhou, Zhengping Wang, and Xinguang Xu**

State Key Laboratory of Crystal Materials, Shandong University, Jinan 250100, China

*DOI: 10.1109/JPHOT.2015.2396905*


Manuscript received January 11, 2015; accepted January 21, 2015. Date of publication January 26, 2015; date of current version February 13, 2015. This work was supported in part by the National Natural Science Foundation of China under Grant 61178060 and in part by the Natural Science Foundation for Distinguished Young Scholar of Shandong Province under Grant 2012JQ18. Corresponding authors: Z. Wang and X. Xu (e-mail: zpwang@sdu.edu.cn; xgxu@sdu.edu.cn).

**Abstract:** In this paper, a new method is used to direct generate Ince–Gaussian (IG) modes from a pulsed solid-state microchip laser. By moving a circular aperture horizontally, the gain size in the laser medium is adjusted, and different IG laser modes are obtained successively. The output laser possesses a stable pulse duration of 500–600 ps; at the same time, the repetition frequency varies between 7 and 16 kHz. To our knowledge, this is the first time that IG modes are obtained in the subnanosecond laser domain, which will be helpful for making large-energy high-peak-power devices.

**Index Terms:** Ince–Gaussian mode, subnanosecond pulse, microchip laser.

## 1. Introduction

Ince–Gaussian (IG) modes, which are a third family of paraxial wave equation solutions, are orthogonal in elliptic coordinates [1]. They can transit into rectangular and cylindrical coordinate solutions, i.e., Hermite–Gaussian modes [2]–[4] and Laguerre-Gaussian modes [5]–[10], by adjusting ellipticity $\varepsilon$ [11]. IG modes have been utilized in form of optical vortices for optical trapping [12], [13], optical tweezers [14], [15], and quantum information tasks [16]. Different methods have been used to generate high order IG modes, including off-axis pumping, tilted pumping, or introducing a crosshair inside the cavity [17]–[19]. Single-frequency and nanosecond pulsed IG mode operations of diode-pumped microchip lasers have been reported previously [17], [20].

Pulsed IG modes especially for sub-nanosecond lasers possess high peak power and low average output power. Such properties can provide high efficiency in manipulating small objects and do less harm to them especially for living objects, like biological cells. In order to get sub-nanosecond pulses from microchip lasers, a traditional gain medium and saturable absorber need to be cut thinner, from the millimeter level to the micrometer level. Tilted pumping, which increases threshold power, will take the risk of the laser component's fragmentation.

In this paper, we report the generation of IG modes in a sub-nanosecond microchip laser. A new method, i.e., moving a circular aperture, is invented to adjust the pump beam, and as many as eight types of IG modes have been observed with stable pulse duration of 500–600 ps.

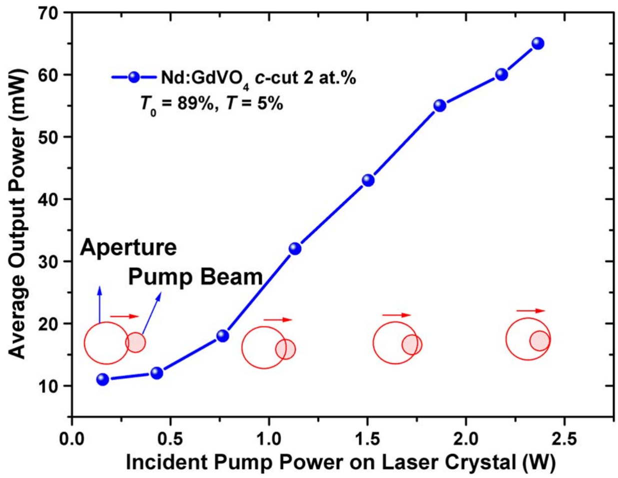


Fig. 1. Average output power versus incident pump power on the $Nd{:}GdVO_4$ microchip.

## 2. Experimental Details

In this experiment, the laser system was a laser diode pumped $Nd{:}GdVO_4/Cr^{4+}$:YAG microchip laser with a plane-parallel cavity. The gain medium was a 0.4 mm thick, c-cut $Nd{:}GdVO_4$ crystal with 2 at.% $Nd^{3+}$ doping, which can generate unpolarized laser. One surface of the $Nd{:}GdVO_4$ crystal was used as the input mirror, which was anti-reflection (AR) coated at 808 nm and high-reflection (HR) coated at 1064 nm. The other surface was AR coated at 1064 nm and HR coated at 808 nm. A 0.2 mm thick, [111]-oriented $Cr^{4+}$:YAG crystal with initial transmission of 89% was used as the passive Q-switcher. One of its surfaces was AR coated at 1064 nm, and the other surface was partial transmission coated at 1064 nm $(\mathrm{T} = 5\%)$, served as the output mirror. The pump source was a commercial available fiber coupled 808 nm laser diodes module (LIMO Inc.). An optical coupler comprised of two lenses delivered the pump light into the laser crystal with a beam radius of 100 $\mu$m. A copper aperture with radius of 0.5 mm was placed ahead of the input mirror. This aperture can be horizontally moved by a slide rail. The Q-switched pulses were detected by a fast photodiode, and measured by a 16-GHz oscilloscope (DSO-X 91604A, Agilent Inc.). The laser output power was measured by an energy/power meter (Power Max 500 D, Molectron Inc.). To record the IG modes, a $KTiOPO_4$ (KTP) crystal cut along the type-II phase-matching direction was used as the frequency doubler to generate green visible laser, then the mode patterns were photographed by a camera (NEX-5N, Sony Inc.)

## 3. Results

Based on the method of Innocenzi *et al.* [21]

$$f = \frac{\pi K_c w_p^2}{P_{ph}(dn/dT)}\left(\frac{1}{1-\exp(-\alpha l)}\right). \tag{1}$$

In (1) with $K_c = 0.0117$ W/mmK, $dn/dT = 4.7 \times 10^{-6}/\mathrm{K}$, $\alpha = 74$ cm$^{-1}$, and $w_p^2/P_{ph} = 0.021$ mm$^2$/W, $l = 0.4$ mm, the thermal lens focal length $f$ was calculated to be 173 mm. Combining with ABCD matrix theory, the fundamental beam radius in the resonator was estimated to be 60 $\mu$m. The incident pump power was set to be 2.37 W. The average pump intensity on laser crystal was calculated to be 75 MW/m$^2$, which was well above the threshold pump intensity of 66 MW/m$^2$. It guaranteed laser could oscillate even at small pump area. To generate IG modes, the circular aperture was moved from surrounding to center with a fixed step length of 25 $\mu$m. Fig. 1 shows the average output power as a function of incident pump power, at different shapes of pump beam. Fig. 2(a) shows the measured intensity distributions of *IG* modes with different mode

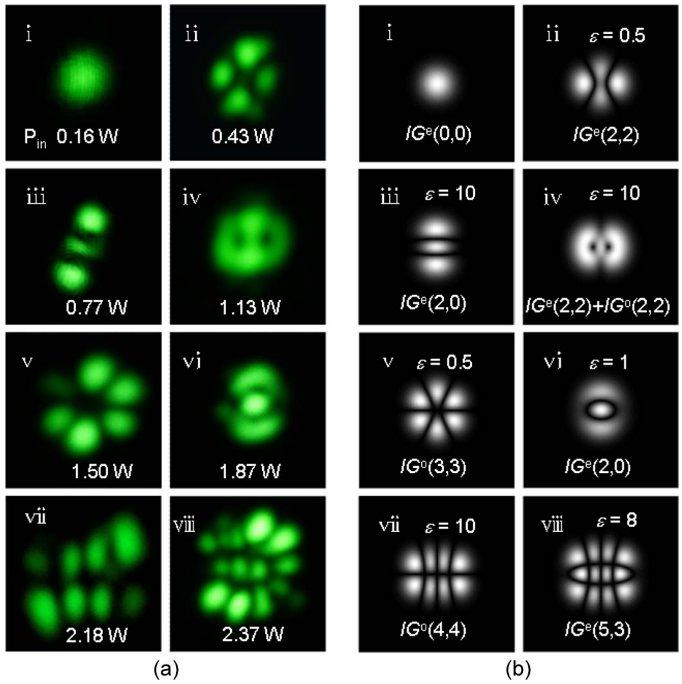


Fig. 2. (a) Intensity distribution of IG modes observed in $Nd{:}GdVO_4/Cr^{4+}$:YAG laser under different incident pump power. (b) Analytical solutions corresponding to the experimental results.

numbers $p$, $m$, and ellipticity $\varepsilon$. The corresponding theoretical simulation results were shown in Fig. 2(b). An $IG^e(0,0)$ mode was observed at an incident pump power of 0.16 W. As the incident pump power increasing, high order $IG$ modes such as $IG^e(2,2)$, $IG^e(2,0)$, $IG^e(2,2)+IG^o(2,2)$, $IG^o(3,3)$, $IG^o(4,4)$, and $IG^e(5,3)$ were obtained successively. In theory, the $IG$ modes in the elliptic coordinate system $r=(\xi,\eta,z)$ are given by [1]

$$IG^e_{p,m}(r,\varepsilon)=\frac{Cw_0}{w(z)}C^m_p(i\xi,\varepsilon)C^m_p(\eta,\varepsilon)\exp\left[-\frac{r^2}{w^2(z)}\right]\times\exp i\left[kz+\frac{kr^2}{2R(z)}-(p+1)\psi(z)\right] \tag{2}$$

$$IG^o_{p,m}(r,\varepsilon)=\frac{Sw_0}{w(z)}S^m_p(i\xi,\varepsilon)S^m_p(\eta,\varepsilon)\exp\left[-\frac{r^2}{w^2(z)}\right]\times\exp i\left[kz+\frac{kr^2}{2R(z)}-(p+1)\psi(z)\right]. \tag{3}$$

The elliptic coordinates are defined in $z$ plane as $x=f(z)\cosh(\xi)\cos(\eta)$, $y=f(z)\sinh(\xi)\times\sin(\eta)$, where $\xi\in[0,\infty)$, $\eta\in[0,2\pi)$, $f(z)=f_0w(z)/w_0$ are the radial and angular elliptic variables, semifocal separation, respectively. $f_0$ is the semifocal separation at the beam waist plane $(z=0)$. $C$ and $S$ are normalized constants. $w(z)$, $w_0$ are the laser beam waists at $z=z$ and $z=0$ planes. $R(z)$ is the phase front curvature radius. $\psi(z)$ is the Gouy shift. $C^m_p$ and $S^m_p$ are different Ince polynomials corresponding to even and odd IG modes, respectively.

The analytical solutions that $m$, $(p-m)/2$ equal number of hyperbolic nodal lines, elliptic nodal lines, with appropriate ellipticity parameter $\varepsilon$ are in agreement with experimental transverse patterns. Due to the saturable absorber ($Cr^{4+}$:YAG), an additional component, and the pump beam profile, smooth connection circular, we find the difficulty of mimicking images by Fresnel-Kirchhoff integration [22]. A qualitative model was derived. The IG modes of Nd: $GdVO_4/Cr^{4+}$:YAG laser were affected by saturated inversion population distribution. According to the analysis of Dong *et al.* [17], the population inversion $\Delta N$ is proportional to the parameter $(P_{in}/\pi w_p^2)\cdot\exp(-2r^2/w_p^2)$. As shown in Fig. 1, when the aperture moved horizontally, the pump intensity $P_{in}/\pi w_p^2$ was controlled to be a constant from first to last, while effective $w_p$ has an increasing tendency for this special pump geometry, and therefore, $\Delta N$ would increase as well.

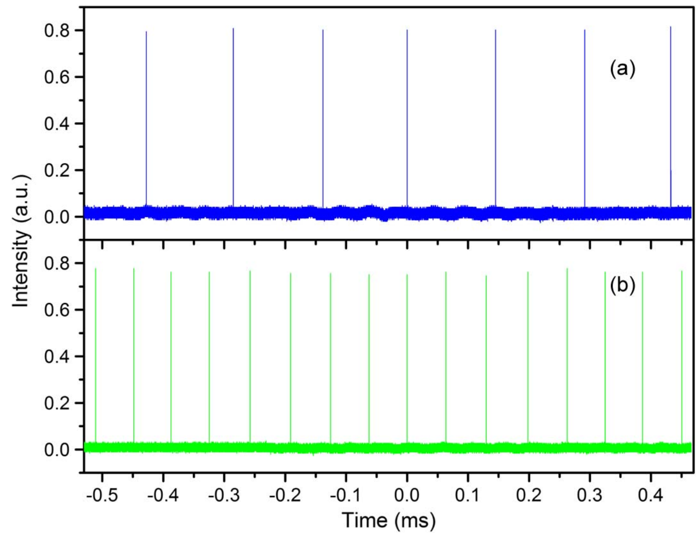


Fig. 3. Pulse trains with repetition frequencies of (a) 7 kHz and (b) 16 kHz for incident pump power of 0.16 W and 2.37 W, respectively.

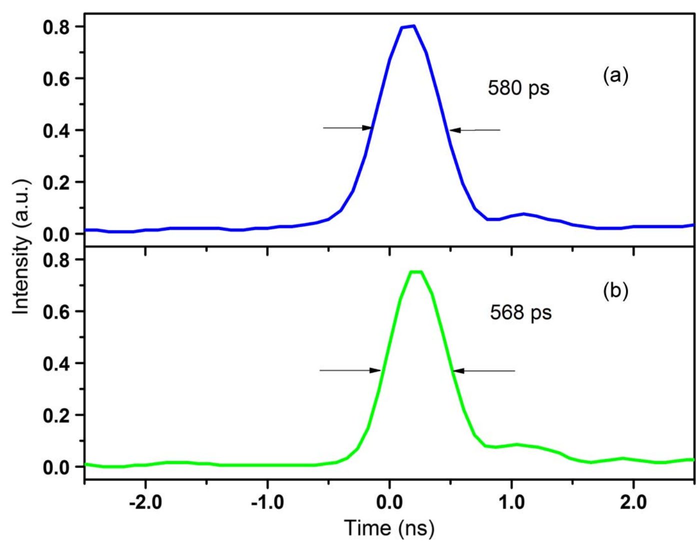


Fig. 4. Pulse profiles with the width of (a) 580 ps and (b) 568 ps for repetition frequencies of 7 kHz and 16 kHz, respectively.

The gain competing in a larger area made high order IG modes oscillating. Meanwhile, the interference pattern of high order IG modes varies slight different from analytical forms due to thermal lens effect with large area. The experiment proved that even and odd modes can be generated through this method.

Figs. 3 and 4 showed the typical pulse trains and profiles of $Nd:GdVO_4/Cr^{4+}$:YAG microchip laser under incident pump power of 0.16, 2.37 W. The laser oscillated at 7 and 16 kHz repetition rates with less than 5% time jitter, which is less than 1% pulse amplitude fluctuation. The pulse width of 580, 568 ps were recorded. Table 1 listed the primary parameters for sub-nanosecond IG mode laser. It could be seen that the pulse widths was sustained in a range of 500–600 ps, which was basically independent with the incident pump power. The peak power and repetition frequency increased from 2.3 kW to 7.4 kW and 7 kHz to 16 kHz, respectively. The optical to

TABLE 1

Characteristic parameters of sub-nanosecond *IG* mode microchip laser

| Incident pump power (W) | 0.16 | 0.43 | 0.77 | 1.13 | 1.50 | 1.87 | 2.18 | 2.37 |
|---|---|---|---|---|---|---|---|---|
| Pump beam area ($10^{-9}m^2$) | 2.13 | 5.73 | 10.27 | 15.07 | 20.00 | 24.93 | 29.07 | 31.40 |
| Average output power (mW) | 11 | 12 | 18 | 32 | 43 | 55 | 60 | 65 |
| Pulse width (ps) | 580 | 568 | 577 | 547 | 588 | 573 | 574 | 568 |
| Repetition frequency (kHz) | 7 | 9 | 10 | 11 | 12 | 13 | 15 | 16 |
| Peak power (kW) | 2.7 | 2.3 | 3.1 | 5.3 | 6.1 | 7.4 | 7.0 | 7.2 |
| *IG* mode | $IG^e(0,0)$ | $IG^e(2,2)$, $\varepsilon = 0.5$ | $IG^e(2,0)$, $\varepsilon = 10$ | $IG^e(2,2)+IG^o(2,2)$, $\varepsilon = 10$ | $IG^o(3,3)$, $\varepsilon = 0.5$ | $IG^e(2,0)$, $\varepsilon = 1$ | $IG^o(4,4)$, $\varepsilon = 10$ | $IG^e(5,3)$, $\varepsilon = 8$ |

optical conversion efficiency $(\eta_{o-o})$ of the fundamental mode, $IG^e(0,0)$, was 6.9%, which was higher than those of high order IG modes (2.3–2.9%).

## 4. Conclusion

By moving a circular aperture to vary the pump area, high peak power, sub-nanosecond IG modes were obtained from a $Nd{:}GdVO_4/Cr^{4+}{:}YAG$ microchip laser. Under an incident pump power of 0.16 W, the $IG^e(0,0)$ mode was generated with an optical to optical efficiency of 6.9%. When incident pump power increased to 2.37 W, $IG^e(5,3)$, $\varepsilon = 8$ mode was obtained with 568 ps pulse duration and 7.2 kW peak power. This high performance, miniature IG laser device will have good application prospects in many scopes, such as quantum cryptography, quantum teleportation, and quantum computation.

## References

[1] M. A. Bandres and J. C. Gutiérrez-Vega, “Ince-Gaussian modes of the paraxial wave equation and stable resonators,” *J. Opt. Soc. Amer. A.*, vol. 21, no. 5, pp. 873–880, May 2004.
[2] S. Chu, Y. Chen, K. Tsai, and K. Otsuka, “Generation of high-order Hermite-Gaussian modes in end-pumped solid-state lasers for square vortex array laser beam generation,” *Opt. Exp.*, vol. 20, no. 7, pp. 7128–7141, Mar. 2012.
[3] Y. F. Chen, T. M. Huang, C. F. Kao, C. L. Wang, and S. C. Wang, “Generation of Hermite-Gaussian modes in fiber-coupled laser-diode end-pumped lasers,” *IEEE J. Quantum Electron.*, vol. 3, no. 6, pp. 1025–1031, Jun. 1997.
[4] Y. F. Chen *et al.*, “Analysis of the effect of pump position on transverse modes in fiber-coupled laser-diode end pumped lasers,” *Opt. Commun.*, vol. 136, no. 5/6, pp. 399–404, Apr. 1997.
[5] N. Barré, M. Romanelli, and M. Brunel, “Role of cavity degeneracy for high-order mode excitation in end-pumped solid-state lasers,” *Opt. Lett.* vol. 39, no. 4, pp. 1022–1025, Feb. 2014.
[6] C. J. Flood, G. Giuliani, and H. M. van Driel, “Preferential operation of an end-pumped Nd:YAG laser in high-order Laguerre-Gauss modes,” *Opt. Lett.*, vol. 15, no. 4, pp. 215–217, Feb. 1990.
[7] D. Lin, J. M. O. Daniel, and W. A. Clarkson, “Controlling the handedness of directly excited Laguerre-Gaussian modes in a solid-state laser,” *Opt. Lett.*, vol. 39, no. 13, pp. 3903–3906, Jul. 2014.
[8] L. Mrrucci, C. Manzo, and D. Paparo, “Optical spin-to-orbital angular momentum conversion in inhomogeneous anisotropic media,” *Phys. Rev. Lett.*, vol. 96, Apr. 2006, Art. ID. 163905.
[9] M. W. Beijersbergen, R. P. C. Coerwinkel, M. Kristensen, and J. P. Woerdman, “Helical-wavefront laser beams produced with a spiral phaseplate,” *Opt. Commun.*, vol. 112, no. 5/6, pp. 321–327, 1994.
[10] N. R. Heckenberg, R. McDuff, C. P. Smith, and A. G. White, “Generation of optical phase singularities by computer-generated holograms,” *Opt. Lett.*, vol. 17, no. 3, pp. 221–223, Feb. 1992.
[11] M. A. Bandres and J. C. Gutiérrez-Vega, “Ince-Gaussian beams,” *Opt. Lett.*, vol. 29, no. 2, pp. 144–146, Jan. 2004.

[12] M. Woerdemann, C. Alpmann, and C. Denz, "Optical assembly of microparticles into highly ordered structures using Ince-Gaussian beams," *Appl. Phys. Lett.*, vol. 98, no. 11, Mar. 2011, Art. ID. 111101.
[13] A. Ashkin, J. M. Dziedzic, J. E. Bjorkholm, and S. Chu, "Observation of a single-beam gradient force optical trap for dielectric particles," *Opt. Lett.*, vol. 11, no. 5, pp. 288–290, May 1986.
[14] L. Paterson *et al.*, "Controlled rotation of optically trapped microscopic particles," *Science*, vol. 292, no. 5518, pp. 912–914, May 2001.
[15] S. Chu, C. Yang, and K. Otsuka, "Vortex array laser beam generation from a Dove prism-embedded unbalanced Mach-Zehnder interferometer," *Opt. Exp.*, vol. 16, no. 24, pp. 19 934–19 949, Nov. 2008.
[16] M. Krenn *et al.*, "Entangled singularity patterns of photons in Ince-Gauss modes," *Phys. Rev. A.*, vol. 87, Jan. 2013, Art. ID. 012326.
[17] J. Dong, J. Ma, Y. Y. Ren, G. Z. Xu, and A. A. Kaminskii, "Generation of Ince-Gaussian beams in highly efficient, nanosecond Cr, Nd:YAG microchip lasers," *Laser Phys. Lett.*, vol. 10, no. 8, Aug. 2013, Art. ID. 085803.
[18] U. T. Schwarz, M. A. Bandres, and J. C. Gutiérrez-Vega, "Observation of Ince-Gaussian modes in stable resonators," *Opt. Lett.*, vol. 29, no. 6, pp. 1870–1872, Aug. 2004.
[19] T. Ohtomo, S. Chu, and K. Otsuka, "Generation of vortex beams from lasers with controlled Hermite- and Ince-Gaussian modes," *Opt. Exp.*, vol. 16, no. 5, pp. 5082–5094, Mar. 2008.
[20] T. Ohtomo, K. Kamikariya, K. Otsuka, and S. Chu, "Single-frequency Ince-Gaussian mode operations of laser-diode-pumped microchip solid-state lasers," *Opt. Exp.*, vol. 15, no. 17, pp. 10 705–10 717, Aug. 2007.
[21] M. E. Innocenzi, H. T. Yura, C. L. Fincher, and R. A. Fields, "Thermal modeling of continuous-wave end-pumped solid-state lasers," *Appl. Phys. Lett.*, vol. 56, no. 19, pp. 1831–1833, May 1990.
[22] S. C. Chu and K. Otsuka, "Numerical study for selective excitation of Ince-Gaussian modes in end-pumped solid-state lasers," *Opt. Exp.*, vol. 15, no. 25, pp. 16 506–16 519, 2007.